JCI insight

NK cell subsets define sustained remission in rheumatoid arthritis

Carl Coyle, … , Rowann Bowcutt, Esperanza Perucha

JCI Insight. 2024. https://doi.org/10.1172/jci.insight.182390.

Resource and Technical Advance In-Press Preview

Graphical abstract

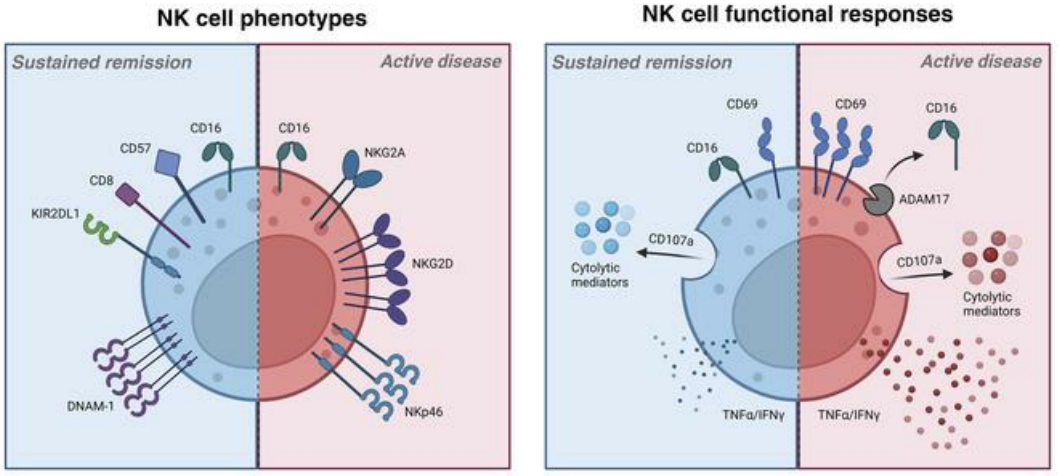

NK cell subsets define sustained remission in rheumatoid arthritis.

Carl Coyle[1,2#], Margaret Ma[2,3,4], Yann Abraham[5], Christopher B. Mahony[6,7], Kathryn Steel[1,2], Catherine Simpson[8], Nadia Guerra[9], Adam P. Croft[6,7], Stephen Rapecki[8], Andrew Cope[1,2], Rowann Bowcutt[8*], Esperanza Perucha[1,2*#].

* Senior co-authors

Corresponding authors

[1] Centre for Inflammation Biology and Cancer Immunology, Floor 1, New Hunt's House, Great Maze Pond, King's College London, Guy's Campus, London, SE1 1UL.

[2] Centre for Rheumatic Diseases, King's College London.

[3] Level 10, Tower Block, Division of Rheumatology, University Medicine Cluster, National University Health System, 1E Kent Ridge Road, 119228, Singapore.

[4] Department of Medicine, National University Singapore, 10 Medical Dr, 117597, Singapore.

[5] Janssen Pharmaceuticals, Turnhoutseweg 30, B-2340 Beerse, Belgium.

[6] Rheumatology Research Group, Institute of Inflammation and Ageing, Queen Elizabeth Hospital, University of Birmingham, Birmingham, UK.

[7] Birmingham NIHR Biomedical Research Centre, University of Birmingham, Birmingham, UK.

[8] UCB Biopharma, 216 Bath Rd, Slough, London, SL1 3WE.

[9] Faculty of Natural Sciences, Department of Life Sciences, Imperial College London

Adress correspondence to: Carl Coyle, Centre for Inflammation Biology and cancer immunology (CIBCI), 1st Floor, New Hunts House, Kings College London, Guys Campus, Great Maze Pond, London SE1 1UL, United Kingdom. Phone: +44 75 35702811; Email: carl.1.coyle@kcl.ac.uk.

Conflict of interests

YA is a current employee of Johnson and Johnson and holds/has access to shares.

RB and CS are current employees of UCB Pharma and hold/have access to shares.

SR is a consultant for Medicxi LLP, director (with shared ownership) in Recycle Bio and Exigent therapeutics and is a paid consultant for Interact Bio.

AC has received consulting and speaker bureau fees from Abbvie, BMS, Galapagos, UCB, Galvani, Janssen, Roche and Arthrogen, and research income in excess of $10,000 from BMS, UCB and Janssen, funds administered by King's College London.

CC, MM, CBM, KS, NG, APC, and EP have no conflicts of interest.

Abstract

Rheumatoid Arthritis (RA) is an immune-mediated, chronic inflammatory condition. With modern therapeutics and evidence-based management strategies, achieving sustained remission is increasingly common. To prevent complications associated with prolonged use of immunosuppressants, drug tapering or withdrawal is recommended. However, due to the lack of tools that define immunological remission, disease flares are frequent, highlighting the need for a more precision medicine-based approach. Utilising high dimensional phenotyping platforms, we set out to define peripheral blood immunological signatures of sustained remission in RA. We identified that $CD8^{+}CD57^{+}KIR2DL1^{+}$ NK cells are associated with sustained remission. Functional studies uncovered an NK cell subset characterized by normal degranulation responses and reduced pro-inflammatory cytokine expression, which was elevated in sustained remission. Furthermore, flow cytometric analysis of NK cells from synovial fluid combined with interrogation of a publicly available single cell RNA-seq dataset of synovial tissue from active RA identified a deficiency of the phenotypic characteristics associated with this NK cell remission signature. In summary, we have uncovered an immune signature of RA remission associated with compositional changes in NK cell phenotype and function that has implications for understanding the impact of sustained remission on host immunity and distinct features which may define operational tolerance in RA.

Graphical Abstract

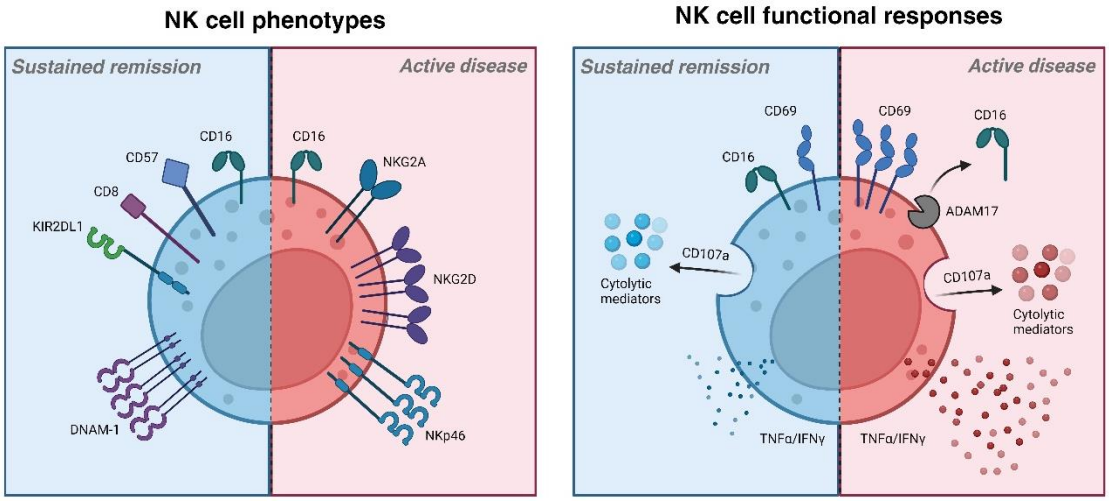

Introduction

Driven by the introduction of more targeted therapeutics and improved clinical management strategies, obtaining clinical remission in patients with RA is now a realistic goal (1). Owing to the complications associated with prolonged immunosuppression(2) clinical management of RA has shifted focus towards optimising strategies for drug dose tapering or, in favourable circumstances, complete drug withdrawal. Despite this ambitious goal, multiple studies to date have described that in the context of drug tapering/withdrawal, disease flare occurs in ~40-50% of patients(3). Whilst this highlights that achieving drug free remission is possible in a subset of patients, the tools to identify these patients are lacking.

Analysis of clinical parameters suggests that lower baseline disease activity and evidence of sustained remission prior to drug tapering is associated with obtaining drug-free remission (4). As such the European Alliance of Associations for Rheumatology recommendations indicate that drug dose tapering should only be considered in patients who demonstrate sustained remission (5). However, evidence shows that residual disease may still be present in some patients achieving clinical remission by even the most stringent criteria (6). Within a subset of patients who achieve sustained clinical remission, residual inflammatory disease will increase the risk of disease flare upon treatment cessation. The failure of clinical disease activity scores to capture the underlying biological heterogenicity of the remission state underscores the urgent need to redefine clinical remission at a molecular and cellular level to uncover biomarkers of sustained deep remission. Such biomarkers could contribute precision medicine approaches in RA routine management.

Studies examining the immunological landscape of sustained clinical remission are limited. However, with the expansion of high dimensional single cell technology combined with multi-omics approaches, data are beginning to emerge (7–12). Integrated results from histological analysis and RNA-seq data have highlighted the heterogeneity of the RA synovial pathotypes and prompted investigations into whether differences in synovial architecture are associated with treatment response and long-term patient outcomes (8, 13). For example, single cell transcriptomic analysis has revealed specific immune subsets associated with sustained remission such as $MerTK^{+}CD206^{+}$ macrophages which promote repair processes in fibroblast like-synoviocytes (7). A recent study identified by mass cytometry that cytotoxic and exhausted $CD4^{+}$ memory T cells, memory $CD8^{+}CXCR5^{+}$ T cells, and $IGHA1^{+}$ plasma cells were associated with disease flares upon treatment cessation (9).

To uncover novel immune signatures of the sustained remission state we undertook an unbiased, cell-agnostic approach, exploiting high dimensional phenotyping technology to profile the immune landscape of RA patients in clinically defined sustained remission derived from the REMission in RA (REMIRA) cohort (14). Our aim was to define remission signatures in the context of peripheral blood as the minimally invasive nature of obtaining such samples should prove advantageous to the feasibility of translating such signatures into clinical practice. Through this approach we have identified key phenotypic and functional subsets of Natural Killer (NK) cells as immune signatures of sustained RA remission. These signatures provide insight into the impact of sustained remission on host defence systems, facilitating the assessment of operational tolerance in RA.

Results

Peripheral blood CD8$^+$CD57$^+$ NK cells are associated with sustained RA remission.

To define immune signatures of sustained RA remission, longitudinal changes in DAS28-CRP scores from the REMission in RA cohort (14) were scrutinised to define differential patient trajectory groups. Individuals who maintained DAS28 remission for a 12-month period were denoted as ‘stable remission’ while individuals who cycled between periods of remission and low to moderate disease activity, suggestive of unstable disease control, were denoted as ‘intermittent remission’ (Figure 1A). To investigate changes in the immune system between remission groups, samples were selected from 5 patients from both groups at timepoints where DAS28 <2.6 (indicating clinical remission) (longitudinal DAS28 scores and selected samples from both groups is detailed in table 1) and stained for mass cytometry immune phenotyping (panel information is detailed in supplementary table 1). Matching samples according to DAS28 remission scores allowed us to compare stable and intermittent remission groups at a time when both were deemed to be in clinical remission, despite longitudinally progressing on two very different clinical trajectories. A summary of participants' demographics, clinical information and treatments are provided in table 2.

Cells with similar phenotypes were automatically grouped using FlowSOM (15), generating 169 clusters, which were manually annotated into metaclusters. A generalised linear mixed model was fit to the data to assess differential cluster abundance between intermittent and stable remission, results of which were integrated into a minimal spanning tree visualization plot (Figure 1B). While results showed fold-change differences in multiple clusters, a collection of clusters corresponding to CD56^{dim} NK cell subsets were

found to be significantly depleted, indicating an increased proportion in these populations in stable remission when compared to intermittent remission.

To identify compositional shifts within $CD56^{dim}$ NK cell subsets between remission groups and identify surface markers which drive these differences we utilised Freeviz analysis (16). Firstly, the data identified that expression intensity of CD57 on $CD56^{dim}$ NK cells was higher in stable remission when compared to intermittent remission (Figure 1C, left panel). Given that CD57 expression is associated with NK cell maturation (17) our data suggested that increased expression of markers of mature NK cell subsets were associated with stable RA remission. Secondly, Freeviz analysis of the $CD57^{+}CD56^{dim}$ NK cell subset demonstrated that expression of CD8 contributed further to the separation of mature $CD57^{+}$ NK cells that distinguished stable from intermittent remission (Figure 1C, right panel), such that the proportion of $CD8^{+}CD57^{+}$ NK cells were significantly increased in stable RA remission (Figure 1D).

To perform a cross-platform validation of our mass cytometry signature, as well as to provide additional phenotypic granularity, we designed an extended NK cell phenotyping panel for spectral flow cytometry on a validation set of samples from the REMIRA cohort. In addition, we included patients with active disease and age matched healthy controls to compare extreme phenotypes. A summary of the demographics, clinical information and treatments for each group is provided in supplementary table 4.

It is interesting to note that while TJC and ESR levels in active disease may be contributing to increased DAS28 scores, the largest difference across groups is reflected in patient reported outcomes. In general, the number of swollen joints and inflammatory markers remained low across groups, suggesting that clinical inflammatory markers were

unable to capture the underlying biological heterogeneity driving different disease outcomes.

First, samples were enriched for NK cells by magnetic depletion of $CD3^+$ and $CD19^+$ lymphocytes and stained using a spectral flow panel as detailed in supplementary table 2. To validate the increased $CD8^+CD57^+$ subsets observed in remission, $CD56^{bright}$ and $CD56^{dim}$ NK cell subsets were first gated based on expression of CD56 and CD16 (Figure 1E), followed by analysis of the co-expression of CD8 and CD57, subdividing total $CD56^{dim}$ NK cells into four discrete subsets. We observed significantly increased proportions of $CD8^+CD57^+$ NK cells in the blood of patients in stable remission when compared to intermittent remission and active disease (Figure 1F), validating the mass cytometry data. While proportions of $CD8^+CD57^+$ NK cells in healthy controls were more variable, median values aligned more to those observed in stable remission. To assess the stability of this NK cell subset in patients in stable remission over time we analysed the proportion of $CD8^+CD57^+$ NK cell subsets in paired samples taken at baseline and after 12 months (Figure 1G). No statistically significant differences were observed between timepoints, suggesting that peripheral blood $CD8^+CD57^+$ NK cells in sustained remission were stable over time.

We noted that the increased frequency of $CD8^+CD57^+$ cells in stable remission was associated with a decrease in the proportion of $CD8^-CD57^-$ NK cells, especially when compared to active disease (Supplementary figure 1A). No differences in the proportion of $CD8^+CD57^-$ and $CD8^-CD57^+$ NK cells were observed across RA disease activity states, although when compared to healthy controls subsets were reduced and increased respectively (Supplementary figure 1B and 1C). Lastly, we found no differences in the

proportion of $CD56^{bright}$ NK cells (Supplementary figure 1D). All together, these data indicated that $CD8^{+}CD57^{+}$ NK cells are expanded in the periphery of RA patients in sustained remission and that this signature is stable over time.

$CD8^{+}CD57^{+}$ NK cells expressing KIR2DL1 are expanded in stable remission.

NK cell surface receptors are commonly classified according to their associated signalling responses as either activating or inhibitory. The fundamental importance of inhibitory receptor signalling in establishing the functional capacity of NK cells, a process referred to as NK cell functional licencing, is underpinned by the hypofunctional state of NK cells lacking expression of inhibitory receptors (18).

To investigate whether the composition of NK cells from stable remission was associated with a specific inhibitory receptor profile, we interrogated the spectral flow cytometry data derived from our validation sample set (detailed in figure 1) to compare the proportion of total $CD56^{dim}$ NK cells expressing NKG2A to those expressing KIR2DL1 (selected as a representative KIR based on evidence suggesting that it has the strongest licensing impact of all KIRs (19, 20)) (Figure 2A). The results demonstrated that for stable remission, like healthy controls, there were equal proportions of $CD56^{dim}$ NK cells expressing both inhibitory receptors, suggesting a more diverse inhibitory receptor profile. In contrast, intermittent remission, like active disease demonstrated a redistribution in inhibitory receptor expression reflected in an increased proportion of $CD56^{dim}$ NK cells preferentially expressing NKG2A.

To assess the contribution of the remission associated $CD8^+CD57^+$ subsets to compositional changes in inhibitory receptor expression, we compared the proportion of these subsets expressing KIR2DL1 to those expressing NKG2A as a percentage of total $CD56^{dim}$ NK cells (Figure 2B). NK cells from healthy controls were composed of greater proportions of $CD8^+CD57^+$ expressing KIR2DL1, consistent with the literature demonstrating an increase in KIR expression associated with $CD57^+$ NK cell subsets (21). In contrast, both intermittent remission and active disease demonstrated increased proportions of $CD8^+CD57^+$ subsets expressing NKG2A, in keeping with the overall expansion of $NKG2A^+$ $CD56^{dim}$ NK cells observed in these groups. Interestingly, NK cells from patients in stable remission were composed of equal proportions of $CD8^+CD57^+$ subsets expressing both inhibitory receptors, suggesting that remission is associated with a more heterogenous pool of this expanded subset. Nonetheless the overall proportion of $CD8^+CD57^+$ NK cells expressing KIR2DL1 was increased in stable remission, particularly when compared to active disease (Figure 2C) allowing us to conclude that $CD8^+CD57^+KIR2DL1^+$ NK cells in peripheral blood are associated with sustained RA remission.

$CD8^+CD57^+$ NK cells display increased levels of CD226 expression consistent across RA disease activity states.

Next, we further interrogated the spectral flow cytometry data derived from our validation sample set to investigate whether $CD8^+CD57^+$ NK cells in stable remission were associated with changes in activating receptor expression. Analysis of the proportion of total $CD56^{dim}$ NK cells expressing NKG2D, NKp46, CD16 and CD226 revealed that more

than 95% of circulating NK cells express each given activating receptor consistent across disease activity states (Supplementary figure 2A) Thus, we investigated whether the levels of receptor expression (as indicated by median fluorescent intensity (MFI)) differed across NK cell subsets subdivided by CD8 and CD57 expression. Our results revealed a differential MFI according to CD57 expression status, with levels of NKG2D and NKp46 significantly reduced within $CD57^+$ NK cells while the expression of CD226 was increased (Figure 3A-C). No differences in the level of CD16 expression was observed (Figure 3D). These differences were not associated with CD8 expression, implying that changes are associated exclusively with differentiation.

Although stable remission was associated with expansion in the overall proportions of $CD8^+CD57^+$ NK cells, CD226 MFI was consistent across the spectrum of RA disease activity (Figure 3E), suggesting that changes in functional capacity are controlled through compositional shifts in the proportion of subsets expressing CD226 rather than changes in the expression at a subset level. This was similar for expression levels of NKG2D, NKp46 and CD16 (Supplementary figure 2B). In conclusion, $CD8^+CD57^+$ NK cells seen in stable remission were defined by lower levels of NKG2D and NKp46, and higher levels of CD226 relative to their $CD57^-$ counterparts.

Degranulation with reduced pro-inflammatory cytokine expression is a functional characteristic of NK cells from stable remission.

Thus far we have identified that the expansion of an NK cell subset in peripheral blood is associated with sustained RA remission. The question arises as to whether changes in NK cell subsets in the blood of remission patients represent solely a biomarker of

treatment response or whether there may also be differences in their functional capacity, suggesting a role for modulation of NK cell effector function in inducing disease remission.

To investigate whether remission is associated with changes in NK cell functionality, we purified NK cells from patients in stable remission, stimulated them for 16hrs with IL-2 to enhance functional responses, and then co-cultured them with K562 target cells prior to analysis by flow cytometry (Figure 4A). Phenotyping panel information is summarised in supplementary table 3. We also included data from healthy controls and active RA disease to compare extreme phenotypes (sample summary information is detailed in supplementary table 5). Cellular activation was evaluated by surface CD69 expression and pro-inflammatory cytokine expression (IFN-γ and TNF-α), while surface expression of CD107a (LAMP-1) was used as a readout for NK cell degranulation.

CD69 expression revealed than in response to IL-2 stimulation and K562 target cell interaction, NK cells from RA patients in stable remission exhibited levels of activation like healthy controls, while NK cells from RA patients with active disease displayed elevated levels of activation (Figure 4B). A similar pattern of response was observed for expression of TNF-α (Figure 4C). Importantly, IFN-γ expressing NK cells were significantly reduced in stable remission when compared to healthy donors, and even lower than those observed in NK cells from patients with active disease (Figure 4D), while surface expression of CD107a did not show any statistically significant differences between groups (Figure 4E). We conclude that NK cells from patients in stable remission retain the capacity for degranulation in response to target cell engagement but produce much lower levels of inflammatory cytokines. In addition, functional responses of $CD56^{bright}$ NK cells revealed no differences in cytokine expression and degranulation

among groups (Supplementary figure 3A-3C), suggesting that reductions in IFN-γ expression in stable remission was specific to the $CD56^{dim}$ NK cell compartment.

To evaluate the co-expression patterns of both pro-inflammatory cytokines and degranulation, Simplified Presentation of Incredibly Complex Evaluations (SPICE) analysis was performed (22). Boolean gating of NK cell proportions based on expression of CD107a, IFN-γ and TNF-α gave rise to 8 distinct functional NK cell subtypes (Figure 4F and Supplementary Figure 4). In response to K562 target cell interaction, NK cells from stable remission exhibited reduced proportions of polyfunctional $CD107a^{+}IFN\text{-}\gamma^{+}TNF\text{-}\alpha^{+}$ subsets (Figure 4G), while proportions of $CD107a^{+}IFN\text{-}\gamma^{-}TNF\text{-}\alpha^{-}$ subsets where significantly increased (Figure 4H), indicating that NK cells from RA patients in remission gained a specific functional subset with intact ability to degranulate in the absence of pro-inflammatory cytokine expression.

Finally, given that co-expression of CD57 and CD8 defined a subset of NK cells that were expanded in the blood of RA patients in stable remission we analysed whether the proportion of $CD107a^{+}IFN\text{-}\gamma^{+}TNF\text{-}\alpha^{+}$ polyfunctional subsets was different between $CD8^{-}$ and $CD8^{+}$ subsets (Supplementary figure 5A) and $CD57^{-}$ and $CD57^{+}$ subsets (Supplementary figure 5B). Consistent across all groups the expression of CD8 was associated with increased polyfunctional NK cells indicating that $CD8^{+}$ NK cells exhibit enhanced effector functions when compared to $CD8^{-}$ subsets. No significant differences in polyfunctional NK cells were observed between CD57- and CD57+ NK cells.

A distinct phenotypic subset associated with in vitro polyfunctional responses is reduced in stable remission.

Given the fundamental link between NK cell subset diversity and functional responses (23), we further interrogated our functional dataset (as detailed in Figure 4) to investigate whether $CD107a^{+}IFN\text{-}\gamma^{+}TNF\text{-}\alpha^{+}$ polyfunctional NK cells (Figure 4G) were associated with a specific in vitro induced phenotypic subset.

Analysis revealed that in response to IL-2 stimulation and K562 target cell interaction, a $CD56^{dim}CD16^{-}$ NK cell subset emerged (Figure 5A). Evidence has shown that in response to activation, surface expression of CD16 on NK cells is reduced, driven by enzymatic cleavage via a Disintegrin and Metalloprotease 17 (ADAM17) (24). We hypothesised that the in-vitro emergence of this $CD56^{dim}CD16^{-}$ subset would occur because of ADAM17-mediated CD16 receptor shedding. To test this, IL-2 stimulated NK cells were co-cultured with K562 cells in the presence of TAPI-0, a known inhibitor of ADAM17 function (Figure 5A). In the presence of inhibitor, the proportion of $CD56^{dim}CD16^{-}$ NK cells were significantly reduced, indicating that TAPI-0 inhibited surface CD16 receptor loss (Figure 5A and B). Furthermore, NK cells from stable remission demonstrated significant reductions in the frequency of $CD56^{dim}CD16^{-}$ NK cell subsets when compared to active RA (Figure 6C), despite no differences in the baseline expression of CD16 (Supplementary figure 6).

Next, we analysed the differences in functional responses of $CD56^{dim}CD16^{-}$ and $CD56^{dim}CD16^{+}$ NK cells to determine if either subset was associated with polyfunctionality. Increased expression of TNF-α, IFN-γ and CD107a was observed in $CD56^{dim}CD16^{-}$ NK cells (Figures 5D-F) resulting in a corresponding increase in

CD107a^{+}IFN-γ^{+}TNF-α^{+} subsets exclusively in CD56^{dim}CD16^{-} NK cells (Figure 5G). No significant differences were observed in the proportion of CD107a^{+}IFN-γ^{-}TNF-α^{-} subsets between CD56^{dim}CD16^{-} and CD56^{dim}CD16^{+} NK cells (Figure 5H). Thus, we can confirm that in response to IL-2 stimulation and K562 target cell interaction, ADAM17 mediated shedding of CD16 gives rise to a CD56^{dim}CD16^{-} NK cell subset which is associated with polyfunctional NK cell responses and that this subset is reduced in RA patients in sustained remission.

Given the importance of inhibitory receptor expression in controlling NK cell effector functions we next investigated whether CD56^{dim}CD16^{-} and CD56^{dim}CD16^{+} NK cells were enriched for subsets expressing specific inhibitory receptors and whether this expression differed when compared to baseline. Significant increases in the proportion of NKG2A^{+} NK cells with a corresponding reduction in the proportion of KIR2DL1^{+} NK cells were observed within CD56^{dim}CD16^{-} NK cells when compared to baseline expression, while no differences in inhibitory receptor expression was observed within CD56^{dim}CD16^{+} NK cells (Figures 5I-K). In addition, we observed a decreased proportion of CD57^{+} NK cells within CD56^{dim}CD16^{-} subset when compared to CD56^{dim}CD16^{+} cells (Figure 5L). These data indicate that CD56^{dim}CD16^{-} NK cells were composed of a predominant NKG2A+KIR-CD57- phenotype, while CD56^{dim}CD16^{+} NK cells have a more diverse repertoire of inhibitory receptor expression which aligned with that of baseline, unstimulated NK cells.

Thus, in response to IL-2 stimulation and K562 target cell interaction ADAM17-mediated shedding of CD16 gives rise to a CD56^{dim}CD16^{-} NK cell subset with a predominant NKG2A+KIR-CD57- phenotype, associated with polyfunctional effector function and inflammatory responses. The corresponding CD56^{dim}CD16^{+} NK cell subset

phenotypically aligned better with baseline unstimulated NK cells while still exhibiting the functional capacity for degranulation in the absence of pro-inflammatory cytokine expression. Furthermore, we demonstrate that such subsets were unevenly represented across RA disease activity states with active disease characterised by a higher proportion of $CD56^{dim}CD16^{-}$ NK cells, while NK cells from stable remission were composed of higher proportions of $CD56^{dim}CD16^{+}$ NK cells.

NK cell subsets associated with stable remission are reduced in inflamed RA joints.

To investigate whether NK cell phenotypes associated with remission are found within inflamed synovial joints, we profiled NK cells from paired peripheral blood (PB) and synovial fluid (SF) of RA patients with active disease (sample summary information is provided in supplementary table 6). The expression of CD56 and CD16 revealed striking differences in the composition of NK cell subsets (Figure 6A) in which SF was enriched in $CD56^{bright}CD16^{-}$ NK cells (Figure 6B) while PB was enriched in $CD56^{dim}CD16^{+}$ NK cells (Supplementary figure 7A). To investigate whether the difference in composition of CD16 negative NK cells between PB and SF could in part be explained by changes in the levels of ADAM17 (given its role in CD16 receptor shedding) we measured the levels of soluble ADAM17 by ELISA in paired serum and synovial fluid samples from active RA patients. Results demonstrate that while we were able to detect appreciable levels of ADAM17, there were no differences observed between serum and fluid samples (Supplementary figure 7B). Thus, the predominant NK cell subset observed in synovial fluid is likely a canonical $CD56^{bright}$ subset (which is inherently CD16 negative) rather than a subset which has undergone CD16 loss. This is further supported by an overlap in the phenotype

of CD56^{bright} NK cells in the fluid with that of those in the blood in terms of CD57, NKG2A and KIR2DL1 expression (Figures 6C-E). This data suggests that CD8^{+}CD57^{+}KIR2DL1^{+} CD56^{dim} NK cell subsets, associated with stable remission, are absent from SF of active RA patients.

To corroborate this observation, we interrogated NK cell signatures from a single cell RNA-seq data set derived from synovial tissue biopsies of active RA patients (25). From the 14 NK cell transcriptional clusters described, we merged clusters corresponding to CD56^{dim} and CD56^{bright} NK cells to generate 8 clusters comprising discrete populations that aligned with our cytometric data (Figure 6F).

Unlike SF, CD56^{dim} NK cells reside in high numbers within synovial tissue, with equal proportions of cells represented in both CD56^{dim} and CD56^{bright} transcriptional clusters (Supplementary figure 7C). However, analysis of *B3GAT1*, the gene encoding CD57, revealed minimal expression within CD56^{dim} NK cells clusters (Figure 6G). Thus, although CD56^{dim} NK cells were found within high numbers in synovial tissue they were predominantly CD57^{-} at a transcriptional level (Figure 6H).

Next, we interrogated the expression of genes encoding NKG2A (*KLRC1*), KIR2DL1 (*KIR2DL1)*, KIR2DL4 (*KIR2DL4*), KIR3DL1 (*KIR3DL1)* and KIR3DL2 *(KIR3DL2)* across CD56^{bright} and CD56^{dim} NK cell clusters (Figure 6I). CD56^{bright} NK cell clusters predominantly expressed *KLRC1* in the absence of genes encoding all KIRs (Figure 6I and Supplementary figure 7D) albeit a select number of patients expressing *KIR2DL4*, the gene encoding a major activating KIR (Supplementary figure 7E). While a small proportion of CD56^{dim} NK cells demonstrated expression of genes encoding *KIR2DL1*, *KIR3DL1* and *KIR3DL2*, a larger proportion of cells expressed *KLRC1* (Figure 6J)

suggesting that the predominant phenotype of $CD56^{dim}$ NK cells within synovial tissue was $NKG2A^{+}KIR^{-}$ at a transcriptional level. Additionally, given our observations regarding preferential expression of KIR2DL1 at the protein level in stable remission we separated samples into those showing greater than or less than 2-fold difference in the number of cells expressing *KLRC1 vs KIR2DL1* (Figures 6K and 6L). We observed that ~75% of synovial tissue samples had higher proportions of $CD56^{dim}$ NK cells expressing *KLRC1.*

Thus, while high numbers of $CD56^{dim}$ NK cells were found within inflamed synovial tissue, their phenotype appears distinct from that in blood, with a predominant $NKG2A^{+}CD57^{-}$ KIR^{-} phenotype. These features align with our in vitro phenotype associated with polyfunctional NK cell effector responses (Figure 5I-5L). We can conclude that NK cell phenotypes associated with RA remission in the blood are reduced from the site of active inflammation in RA.

Discussion

Variable outcomes associated with drug tapering and withdrawal in RA patients highlights the need for a more precision-medicine based approach. Here, we performed unbiased, high dimensional immune phenotyping and identified $CD8^{+}CD57^{+}$ $CD56^{dim}$ NK cells as a novel and distinctive peripheral blood signature associated with stable remission. NK cells, alongside type 1 innate lymphoid cells (ILC1s), are members of a group of innate immune cells referred to as group 1 ILCs (26). ILC subsets are innate immune system effectors which are of lymphoid origin but lack expression of somatically rearranged T or B cell antigen receptors. Group 1 ILCs are defined based on their shared requirement for T-bet expression to promote their development as well as functional overlap in the expression of cytotoxic mediators and IFN-γ (27).

Similar NK cell phenotypes associated with favourable disease outcomes have been reported in the literature, such as $CD8^{+}CD57^{+}$ NK cells associated with slower HIV-1 disease progression (28), a $CD8^{+}$ NK cell transcriptomic signature associated with periods of remission in relapsing remitting multiple sclerosis (29) and $CD8^{+}$ NK cells associated with response to anti-TNF-α therapy in ankylosing spondylitis (30). Thus, it is likely that NK cells may represent a conserved signature of disease remission across multiple disease settings.

We have identified that blood derived $CD56^{dim}$ NK cells in stable remission exhibited increased expansions of $CD8^{+}CD57^{+}$ NK cells expressing KIR2DL1. The fundamental importance of inhibitory receptor expression for inducing NK cell effector functionality is reflected in the hyporesponsive state of NK cells lacking either NKG2A or KIR (18). Differences in both the type and level of expression of KIRs, underpinned by genetic

diversity, has been implicated in disease processes, likely due to variability in different KIRs to promote the functional capacity of NK cell subsets (31). Whether expression of KIR2DL1 contributes to the emergence of a functional subset capable of maintaining disease remission in RA remains to be addressed. Furthermore, we also observed that $CD56^{dim}$ NK cells from healthy controls exhibited expansions of $CD8^{+}CD57^{+}$ NK cells preferentially expressing KIR2DL1 while $CD8^{-}CD57^{-}$ NK cells preferentially expressed NKG2A (data not shown). This is in keeping with the literature which demonstrates that changes in the expression of inhibitory receptors are linked to NK cell differentiation (17), such that $CD57^{-}$ NK cells have higher NKG2A expression while $CD57^{+}$ NK cells express higher levels of KIR. The increased NKG2A expressing $CD57^{+}$ NK cells in intermittent remission and active disease suggests that in the context of KIR2DL1 expression this association was lost. However, it is worth noting that due to the limited coverage of KIRs used in this study, increased proportions of NKG2A expressing $CD8^{+}CD57^{+}$ NK cells associated with reduced $KIR2DL1^{+}$ subsets may reflect the presence of alternatively expressed KIRs. Additional extended KIR phenotyping would enable an investigation of whether alternative KIRs are present within more active clinical states.

In vitro functional assessment revealed that that in response to IL-2 stimulation and K562 target cell interaction, $CD56^{dim}$ NK cells from RA patients in stable remission exhibit a reduction in inflammatory cytokine expression and reduced proportions of polyfunctional NK cell responses. We have also demonstrated that ADAM17-mediated shedding of CD16 gave rise to a $CD56^{dim}CD16^{-}$ subset associated with polyfunctional responses, which was reduced from individuals in stable remission. ADAM17-mediated modulation of CD16 receptor expression has been described as a key NK cell immune checkpoint,

acting as a negative regulator of the effector functions of activated NK cells (32). Indeed, inhibition of ADAM17 has been shown to result in enhanced NK cell functional responses (33). Therefore, CD16 surface shedding corroborates the increased activation state of polyfunctional NK cells observed in active RA while the reduced levels of shedding observed in remission may suggest a more regulated effector response. Increased proportions of $CD107a^{+}TNF\text{-}\alpha^{-}IFN\text{-}\gamma^{-}$ subsets were associated with sustained remission suggesting a predominant functional subtype characterised by degranulation in the absence of pro-inflammatory cytokine expression. Such functionality, which we have coined 'silent degranulation', could be considered advantageous in the context of disease remission by maintaining NK cell degranulation responses, thereby contributing to homeostatic immune surveillance, while restraining the pro-inflammatory burden. Identifying the molecular mechanism controlling cytokine suppression in NK cells from stable remission is an area of further research with the potential for high translational impact, especially if this turns out to be a fundamental control mechanism common to multiple disease entities.

Given the increased proportion of $CD8^{+}CD57^{+}$ NK cells in stable remission, a key question arises as to what extrinsic factors could contribute to the emergence of this subset. While regulation of $CD8^{+}$ NK cell populations remain poorly understood, evidence supports chronic viral infection, particularly human cytomegalovirus (HCMV) infection, as one of the best recognised clinical scenarios associated with expansion of $CD57^{+}$ NK cell subsets (34). Indeed, the host response to HCMV infection has been associated with the expansion of a specialized NK cell subset with adaptive features defined phenotypically by elevated levels of CD57, as well as the expression of the activating receptor NKG2C,

although subsets with similar adaptive like features not expressing NKG2C have been reported (35). Thus, one could hypothesise that $CD8^+CD57^+$ NK cells in stable remission represent a key immune cell subset with intact homeostatic defence systems to control latent viral infection, whose reactivation is associated with disease flares. This raises the intriguing possibility that $CD8^+CD57^+$ NK cells could be more than just a signature of stable remission but could be actively contributing to a sustained remission state.

The role of NK cell cytotoxicity in mediating regulation of adaptive immune responses, in particular modulation of $CD4^+$ and $CD8^+$ T cell responses could also represent a mechanism whereby NK cells could contribute to immune homeostasis (36). Defining whether NK cells in stable remission with the capacity for 'silent degranulation' could contribute to controlling expansion of autoreactive T cells without the release of pro-inflammatory cytokines would be worthy of further investigation. Alternatively, NK cells have been found to reside in high numbers within lymph nodes whereby they modulate dendritic cell function (37), indicating that remission-associated NK cell subsets could regulate autoimmunity by influencing autoantigen presentation in secondary lymphoid organs. Direct crosstalk between NK cells and fibroblast-like synoviocytes has also been documented (38) indicating a potential role for NK cell mediated clearance of these pathogenic stromal cells.

Whether NK cell regulation would occur in the inflamed joint or alter the immune response at an alternative anatomical location would also require addressing. We have shown that NK cells within the joint of active RA are phenotypically distinct (at both the protein and transcriptional level) from our $CD8^+CD57^+KIR2DL1^+$ remission signature, indicating the absence of potential regulatory components. Given that the expression of CD57 is

associated with a reduced proliferative rate and decreased responsiveness to cytokine stimulation (39) we hypothesise that the reduced presence of $CD57^+$ NK cells in the RA joint might be explained by their failure to differentiate in an inflamed microenvironment. In this inflammatory setting, chronic cytokine stimulation would favour the accumulation of $NKG2A^+KIR^-CD57^-$ NK cell phenotypes owing to the increased proliferative rate and enhanced metabolic fitness associated with NKG2A expression (40). This provides further incentives to define pathways for therapeutic control of inflammation within the RA joint which may permit $CD8^+CD57^+$ NK cells to differentiate and induce disease remission. Lastly, given that remission in this study is maintained by treatment, there remains a need to examine the dynamics of these subsets in the context of treatment tapering/withdrawal to investigate whether these NK cell subsets are maintained in drug free remission.

Methods

Sex as a biological variable

Human samples were included from both female and male subjects. A higher proportion of samples from female subjects were included in each group to reflect the increased prevalence of rheumatoid arthritis observed in females.

Study samples

All samples for mass cytometry analysis (Figure 1A-D), stable remission, intermittent remission, and active disease samples for spectral flow cytometry (Figure 1E-G, Figure 2, and Figure 3) and stable remission samples from functional studies (Figure 4 and Figure 5) were derived from the REMission In RA (REMIRA) cohort. RA participants were recruited to the REMIRA study if they were diagnosed according to the 1987 revised American College of Rheumatology criteria. Specific inclusion criteria included: Disease duration of <10 years, stable DMARD treatment for >6 months and a DAS28 score of <3.2 for a least one month before recruitment.

Active disease samples from functional studies (Figure 4 and Figure 5), paired peripheral blood and synovial fluid samples (Figure 6) and all healthy controls were derived from the METAbolic Control of the Immune Response (METACIR) study. RA participants (>18 years old) were recruited to the METACIR study after fulfilling the 2010 ACR/EULAR classification criteria for diagnosis of RA.

Cell isolation

Peripheral blood mononuclear cells (PBMCs) and synovial fluid mononuclear cells (SFMCs) were isolated by density gradient centrifugation using Lymphoprep (Axis-Shield). PBMC from the REMIRA study were cryopreserved in freezing medium containing 10% DMSO (Sigma) in 90% human AB serum (PAA), while PBMC and SFMC from the METACIR study were cryopreserved in freezing medium containing 10% DMSO (Sigma) in 90% foetal bovine serum (Sigma). All samples were stored in liquid nitrogen. Cell viability was routinely tested by Trypan Blue exclusion, with a viability of >85% considered acceptable.

Mass Cytometry staining and acquisition.

After thawing, dead cells were removed from samples using a dead cell removal kit (Miltenyi Biotech) according to manufacturer's instructions. For subsequent wash steps, unfixed cells were washed at 300g for 5 mins and fixed cells at 800g for 5 mins at room temperature (RT). ~3 x 10^6 cells were stained with cisplatin (for live/dead discrimination) (StandardBioTools) in plain RPMI-1640 (Gibco) for 5 mins at RT and washed using RPMI-1640 (Gibco) supplemented with 10% Foetal bovine serum (Sigma) to quench. Cells resuspended in maxpar staining buffer (MSB) (StandardBioTools) were incubated with human FC block (Biolegend) for 10 mins at RT followed immediately by addition of surface stain antibodies (Supplementary table 1), incubated for 60 minutes at RT. Cells were then fixed and barcoded using the Cell-ID 20-Plex Pd barcoding kit (StandardBioTools) according to manufactures instructions. Barcoded cells from multiple samples were pooled and incubated overnight with Cell-ID™ Intercalator-Ir (Fluidigm) prepared at a

1:500 dilution using 2% PFA. Cells were washed twice with PBS and resuspend in 1ml of freezing medium (10% FCS/DMSO) and stored at -80°C until acquisition.

For acquisition, samples were washed with PBS and resuspended in Maxpar CAS buffer (Fluidigm) with EQ Element Calibration Beads (Fluidigm) and acquired on a Helios mass cytometer (Fluidigm).

Flow cytometric analysis.

For wash steps, unfixed cells were washed at 300g for 5 mins and fixed cells at 800g for 5 mins at 4°C unless otherwise stated. Cells were stained with Fixable Viability Dye eFluor™ 455UV (eBioscience™) for 15 mins at 4°C, followed by surface staining for 20 mins at 4°C. For intracellular staining cells were fixed using the Foxp3 / Transcription factor staining buffer set (eBioscience™) according to the manufactures instructions and incubated with intracellular antibodies for 30 mins at 4°C. Cells were washed and resuspended in FACS buffer for acquisition. FCS files were acquired on a Cytek Aurora spectral flow cytometer and analysed using FlowJo (TreeStar).

Where indicated PBMC samples were enriched for NK cells by depletion of $CD3^+$ and $CD19^+$ lymphocytes prior to staining. Cells were incubated with 0.25μg of both biotin anti-human CD3 and biotin anti-human CD19 (Both Biolegend) followed by magnetic depletion using Dynabeads™ Biotin Binder (Thermofisher).

NK cell degranulation assays.

NK cells were purified from PBMCs by negative isolation using an NK cell isolation kit (Miltenyi Biotech). The quality of purification was accessed by measuring the proportion

of NK cells after magnetic isolation by flow cytometry. All samples displayed a purity of >95%. 1 x 10^5 purified cells were cultured in complete media (RPMI-1640 (Gibco) supplemented with 10% foetal bovine serum, 1x glutaMAX (Thermofisher) and 1% Penicillin/Streptomycin) only or complete media in the presence of 200 Uml^{-1} of recombinant human IL-2 (Proleukin, Novartis) for ~18hrs at 37°C and 5% CO_2. After incubation cells were equally split into two wells (~5 x 10^4 per well) to perform stimulations in duplicate. For target cell stimulation, 2 x10^4 K562 cells (kindly donated by Dr. S. Papa, King's college London) were added (E:T ratio of 2.5:1). Brefeldin A and Monensin (both Biolegend) were added (1:1000 dilution) in addition to anti-human CD107a (1:200 dilution) and cells were incubated for 4 hrs at 37°C and 5% CO_2. Where indicated 5μm TAPI-0 (kindly donated by Dr. A. Ivetic) was additionally added to each well and incubated for 4 hrs at 37°C and 5% CO_2. Following incubation cells from duplicate wells were combined and harvested into 5ml FACS tubes for flow cytometry.

Mass cytometry data analyses.

EQ element calibration beads were used for signal intensity normalisation as previously described (41). Barcode signals were deconvoluted using the Fluidigm CyTOF software generating induvial sample FCS files. Data pre-processing was performed using manual gating in FlowJo (TreeStar) as previously described (42). Data quality was assessed by inspecting for technical outliers using HilbertSimilarity (43), where similarity between samples is estimated based on composition No outlier batches were detected using the `outliers.ranking` method (44) with a threshold value of 0.7. Quality checked cells were clustered using FlowSOM into 169 clusters which were manually annotated into

metaclusters by visual inspection of marker expression profiles. The Euclidian distance between clusters was calculated and used to construct a minimal spanning tree graph for visualisation of generated clusters. Differential cluster abundance was performed using a generalised linear mixed model based on *N ~ Condition + Gender +offset(Log(Total))*, where *N* refers to the number of cells in the cluster and *Condition* refers to what clinical state cells were derived from. The term *offset(Log(Total)* was used to account for differences in the number of cells across samples. Lastly, to identify compositional shifts within clusters between clinical states and identify surface markers which drive these differences we utilised the Freeviz method implemented in the Radviz R package as previously reported (45).

Graphics and statistical analysis.

Graphical abstract was created with Biorender.com. For flow cytometry statistical analysis was performed using GraphPad prism. Mann-Whitney tests were performed on two-way comparisons. For multiple groups the Kruskal-Wallis test was performed with Dunns multiple comparison test applied for adjusted p-values. Paired data was analysed with the Wilcoxon matched-pairs signed rank test. A significance threshold of <0.05 was applied throughout the manuscript.

Study approval.

The REMIRA study was approved by the Wandsworth Research Ethics committee (REC:09/H0803/154) and the METACIR study was approved by the London Bloomsbury research committee (REC:18/LO/0399). Both studies were conducted

according to the guidelines of the declaration of Helsinki with written informed consent obtained for all patients.

Data availability.

All raw data and associated code are available from corresponding authors on request. As per the original publication (25) CITE-seq single-cell expression matrices and sequencing are available on Synapse (https://doi.org/10.7303/syn52297840).

Values for data points shown in figures are reported in the Supporting Data Values file.

Author contributions

CC designed, performed, and analysed the experiments and prepared the manuscript. MM and APC conceived and ran the REMIRA study. YA, CBM and APC provided bioinformatic support and contributed to experimental design and preparation of the manuscript. CS provided mass cytometry acquisition support and contributed to experimental design and manuscript preparation. KS and NG contributed to experimental design and preparation of manuscript. SR, AC, RB, and EP conceived the project, designed experiments, supervised research, and contributed to the manuscript preparation.

Acknowledgements

We thank all healthy donors and patients for participation and donation of samples. This research was supported by Research and Development, Guy's and St Thomas' NHS Foundation Trust. The views expressed are those of the author(s) and not necessarily those of the NHS". The authors wish to acknowledge the support of the South Kensington Flow Cytometry Facility at Imperial College London. This research was funded/supported by the EU/EFPIA Innovative Medicines Initiative 2 Joint Undertaking RTCure (777357). UCB Pharma funded a PhD studentship for CC as part of the EU/EFPIA Innovative Medicines Initiative 2 Joint Undertaking RTCure. An NIHR Doctoral Research Fellowship (NIHR/DRF/2009/02/086) was awarded to MM for the REMIRA study. EP acknowledges funding from The Academy of Medical Sciences (SBF007\100069).

References

1. Brown A PM, Isaacs B JD. Rheumatoid arthritis: from palliation to remission in two decades. *Clinical Medicine*. 2014;14(6):50–55.

2. Hamed KM, et al. Overview of Methotrexate Toxicity: A Comprehensive Literature Review. Cureus. 2022;14(9)

3. Verstappen M, van der Helm-van Mil AHM. Sustained DMARD-free remission in rheumatoid arthritis - about concepts and moving towards practice. Joint Bone Spine. 2022;89(6):105418.

4. D'Onofrio B, et al. Inducibility or predestination? Queries and concepts around drug-free remission in rheumatoid arthritis [preprint]. *Expert Rev Clin Immunol*. 2023;19(2):217–225.

5. Smolen JS, et al. EULAR recommendations for the management of rheumatoid arthritis with synthetic and biological disease-modifying antirheumatic drugs: 2019 update. Ann Rheum Dis. 2020;79(6):685-699.

6. Aletaha D, Smolen JS. Remission in rheumatoid arthritis: missing objectives by using inadequate DAS28 targets. Nat Rev Rheumatol. 2019;15(11):633-634.

7. Alivernini S, et al. Distinct synovial tissue macrophage subsets regulate inflammation and remission in rheumatoid arthritis. *Nat Med*. 2020;26(8):1295–1306.

8. Dennis G, et al. Synovial phenotypes in rheumatoid arthritis correlate with response to biologic therapeutics. *Arthritis Res Ther*. 2014;16(2).

9. Baker KF, et al. Single-cell insights into immune dysregulation in rheumatoid arthritis flare versus drug-free remission. *Nat Commun*. 2024;15(1):1063.

10. Tasaki S, et al. Multi-omics monitoring of drug response in rheumatoid arthritis in pursuit of molecular remission. *Nat Commun*. 2018;9(1).

11. Burgoyne CH, et al. Abnormal T cell differentiation persists in patients with rheumatoid arthritis in clinical remission and predicts relapse. *Ann Rheum Dis*. 2008;67(6):750–757.

12. Ma MHY, et al. A multi-biomarker disease activity score can predict sustained remission in rheumatoid arthritis. *Arthritis Res Ther*. 2020;22(1).

13. Humby F, et al. Synovial cellular and molecular signatures stratify clinical response to csDMARD therapy and predict radiographic progression in early rheumatoid arthritis patients. Ann Rheum Dis. 2019;78(6):761-772.

14. Ma MHY, et al. Variable impacts of different remission states on health-related quality of life in rheumatoid arthritis. Clin Exp Rheumatol. 2018;36(2):203-209.

15. Van Gassen S, et al. FlowSOM: Using self-organizing maps for visualization and interpretation of cytometry data. Cytometry A. 2015;87(7):636-645.

16. Demsar J, et al. FreeViz--an intelligent multivariate visualization approach to explorative analysis of biomedical data. J Biomed Inform. 2007;40(6):661-671.

17. Lopez-Vergès S, et al. CD57 defines a functionally distinct population of mature NK cells in the human CD56dimCD16+ NK-cell subset. Blood. 2010;116(19):3865-3874.

18. Anfossi N, et al. Human NK cell education by inhibitory receptors for MHC class I. Immunity. 2006;25(2):331-342.

19. Hilton HG, et al. Polymorphic HLA-C Receptors Balance the Functional Characteristics of KIR Haplotypes. J Immunol. 2015;195(7):3160-3170.

20. Chapel A, et al. Peptide-specific engagement of the activating NK cell receptor KIR2DS1. Sci Rep. 2017;7(1):2414.

21. Béziat V, et al. NK cell terminal differentiation: correlated stepwise decrease of NKG2A and acquisition of KIRs. PLoS One. 2010;5(8):e11966.

22. Roederer M, Nozzi JL, Nason MC. SPICE: exploration and analysis of post-cytometric complex multivariate datasets. Cytometry A. 2011;79(2):167-174.

23. Cheent K, Khakoo SI. Natural killer cells: integrating diversity with function. Immunology. 2009;126(4):449-457.

24. Romee R, et al. NK cell CD16 surface expression and function is regulated by a disintegrin and metalloprotease-17 (ADAM17). Blood. 2013;121(18):3599-3608.

25. Zhang F, et al. Deconstruction of rheumatoid arthritis synovium defines inflammatory subtypes. Nature. 2023;623(7987):616-624.

26. Spits H, Cupedo T. Innate lymphoid cells: emerging insights in development, lineage relationships, and function. Annu Rev Immunol. 2012;30:647-675.

27. Hazenberg MD, Spits H. Human innate lymphoid cells. Blood. 2014;124(5):700-709.

28. Ahmad F, et al. High frequencies of polyfunctional CD8+ NK cells in chronic HIV-1 infection are associated with slower disease progression. J Virol. 2014;88(21):12397-12408.

29. McKinney EF, et al. A CD8+ NK cell transcriptomic signature associated with clinical outcome in relapsing remitting multiple sclerosis. Nat Commun. 2021;12(1):635.

30. Schulte-Wrede U, et al. An explorative study on deep profiling of peripheral leukocytes to identify predictors for responsiveness to anti-tumour necrosis factor alpha therapies in ankylosing spondylitis: natural killer cells in focus. Arthritis Res Ther. 2018;20(1):191.

31. Kulkarni S, Martin MP, Carrington M. The Yin and Yang of HLA and KIR in human disease. Semin Immunol. 2008;20(6):343-352.

32. Wu J, Mishra HK, Walcheck B. Role of ADAM17 as a regulatory checkpoint of CD16A in NK cells and as a potential target for cancer immunotherapy. J Leukoc Biol. 2019;105(6):1297-1303.

33. Pham DH, Kim JS, Kim SK, et al. Effects of ADAM10 and ADAM17 Inhibitors on Natural Killer Cell Expansion and Antibody-dependent Cellular Cytotoxicity Against Breast Cancer Cells In Vitro. Anticancer Res. 2017;37(10):5507-5513.

34. Lopez-Vergès S, et al. Expansion of a unique $CD57^{+}$NKG2Chi natural killer cell subset during acute human cytomegalovirus infection. Proc Natl Acad Sci U S A. 2011;108(36):14725-14732.

35. Della Chiesa M, et al. Human cytomegalovirus infection promotes rapid maturation of NK cells expressing activating killer Ig-like receptor in patients transplanted with NKG2C-/- umbilical cord blood. J Immunol. 2014;192(4):1471-1479.

36. Schuster IS, et al. "Natural Regulators": NK Cells as Modulators of T Cell Immunity. Front Immunol. 2016;7:235.

37. Degli-Esposti MA, Smyth MJ. Close encounters of different kinds: dendritic cells and NK cells take centre stage. Nat Rev Immunol. 2005;5(2):112-124.

38. Chan A, et al. Mediation of the proinflammatory cytokine response in rheumatoid arthritis and spondylarthritis by interactions between fibroblast-like synoviocytes and natural killer cells. Arthritis Rheum. 2008;58(3):707-717.

39. Nielsen CM, et al. Functional Significance of CD57 Expression on Human NK Cells and Relevance to Disease. Front Immunol. 2013;4:422.

40. Highton AJ, et al. High Metabolic Function and Resilience of NKG2A-Educated NK Cells. Front Immunol. 2020;11:559576.

41. Finck R, et al. Normalization of mass cytometry data with bead standards. Cytometry A. 2013;83(5):483-494.

42. Iyer A, Hamers AAJ, Pillai AB. CyTOF® for the Masses. Front Immunol. 2022;13:815828.

43. Abraham, Y.and M. Neri. Hilbertsimilarity : Estimating Sample Similarity in Single Cell High Dimensional Datasets. 0.4.3, Zenodo, 12 Nov. 2019, https://zenodo.org/records/3557362

44. Torgo L. *Data Mining using R: learning with case studies*. Chapman & Hall/CRC; 2016.

45. Yann Abraham. Yannabraham/radviz: Interactive Visualizations and Better Scaling. 0.9.3, Zenodo, 28 Mar. 2022, https://zenodo.org/records/6388588

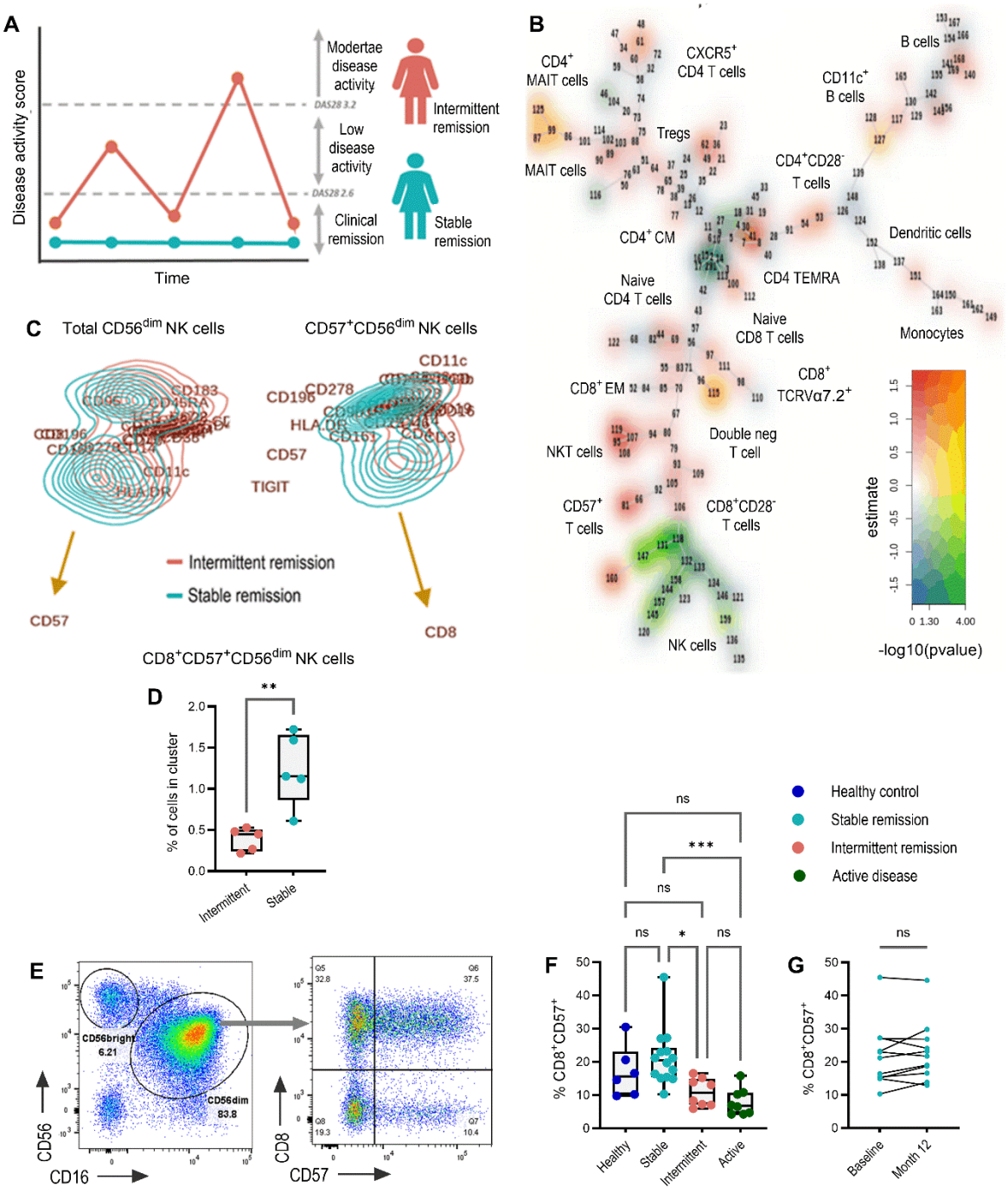
A
Disease activity score
Time
Modertae disease activity
DAS28 3.2
Low disease activity
DAS28 2.6
Clinical remission
Intermittent remission
Stable remission
B
CD4+ MAIT cells
CXCR5+ CD4 T cells
B cells
CD11c+ B cells
Tregs
MAIT cells
CD4+CD28- T cells
CD4+ CM
Dendritic cells
Naive CD4 T cells
CD4 TEMRA
Naive CD8 T cells
Monocytes
CD8+ EM
CD8+ TCRVα7.2+
Double neg T cell
NKT cells
CD57+ T cells
CD8+CD28- T cells
NK cells
estimate
-log10(pvalue)
C
Total CD56dim NK cells
CD57+CD56dim NK cells
CD183
CD45RA
CD196
CD278
CD11c
HLA DR
CD161
CD3
CD57
TIGIT
Intermittent remission
Stable remission
CD57
CD8
CD8+CD57+CD56dim NK cells
D
% of cells in cluster
Intermittent
Stable
E
CD56bright
6.21
CD56dim
83.8
CD56
CD16
CD8
CD57
F
% CD8+CD57+
Healthy
Stable
Intermittent
Active
Healthy control
Stable remission
Intermittent remission
Active disease
G
% CD8+CD57+
Baseline
Month 12

Figure 1. Peripheral blood $CD8^{+}CD57^{+}$ NK cells are associated with sustained RA remission. (A) Longitudinal changes in DAS28 scores define key patient trajectory groups, (B) Multiple spanning tree visualisation depicting differential cluster abundance analysis (comparing intermittent to stable remission) according to differences in fold change (color gradient along the y-axis) and in order of increasing significance (color gradient along the x-axis), (C) Freeviz analysis comparing total $CD56^{dim}$ NK cells (left) and Total $CD56^{dim}CD57^{+}$ NK cells (right), (D) The Percentage of cells in $CD8^{+}CD57^{+}$ NK cell clusters between intermittent (n=5) and stable remission (n=5), (E) Flow cytometry gating to define $CD56^{dim}$ NK cells (left) followed by sub setting based on CD8 and CD57 expression (right), (F) The proportion of $CD8^{+}CD57^{+}$ $CD56^{dim}$ NK cells across healthy donors (n=6), stable remission (n= 14), intermittent remission (n=8) and active disease (n=8), (G) The proportion of $CD8^{+}CD57^{+}$ NK cells from paired baseline and month 12 samples from stable RA remission (n=10). Whiskers on plots represent min to max values. P values were determined by using the Mann Whitney test (D), Kruskal-Wallis test with Dunns multiple test correction (F) and Wilcoxon matched-pairs signed rank test (G). *P <0.05, **P <0.01, P*** <0.001.

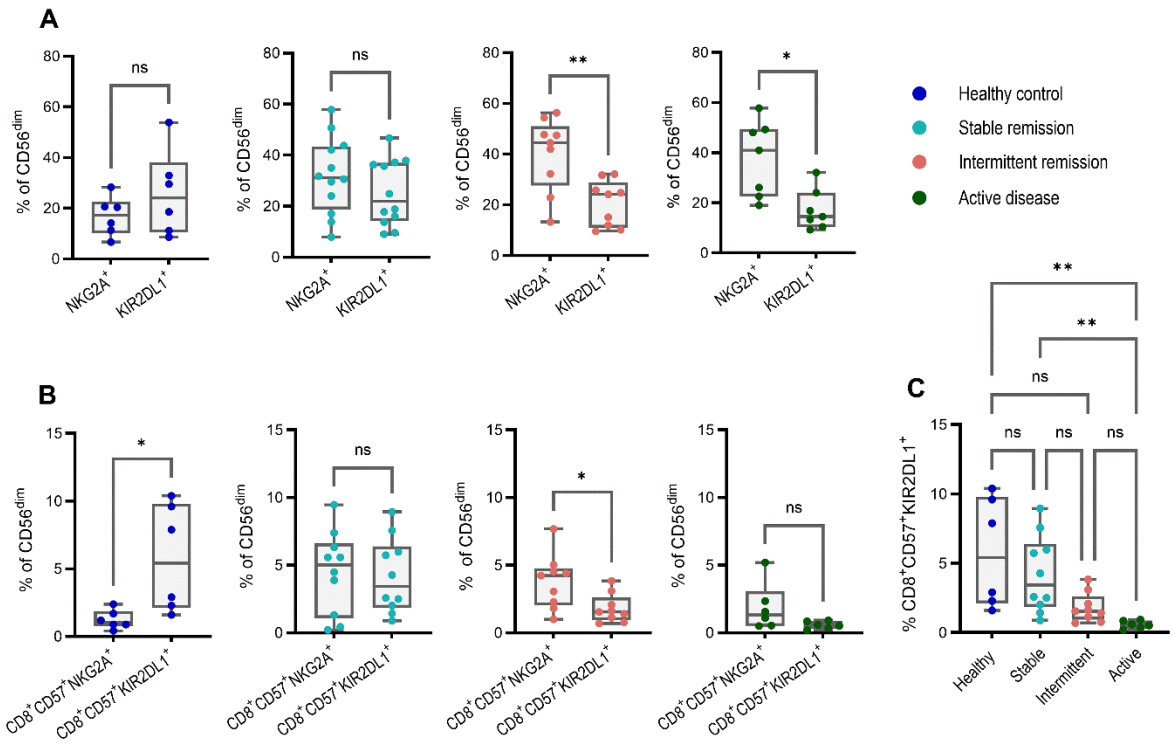

Figure 2. $CD8^{+}CD57^{+}$ NK cells expressing KIR2DL1 are expanded in stable remission. (A) the proportion of total $CD56^{dim}$ NK cells which are $NKG2A^{+}$ compared to $KIR2DL1^{+}$, (B) The proportion of total $CD56^{dim}$ NK cells which are $CD8^{+}CD57^{+}NKG2A^{+}$ compared to $CD8^{+}CD57^{+}KIR2DL1^{+}$, (C) $CD8^{+}CD57^{+}KIR2DL1^{+}$ NK cells as a percentage of $CD56^{dim}$. Whiskers on plots represent min to max values. P values were determined by using the Mann Whitney test (A-B) and Kruskal-Wallis test with Dunns multiple test correction (C). *P <0.05, **P <0.01.

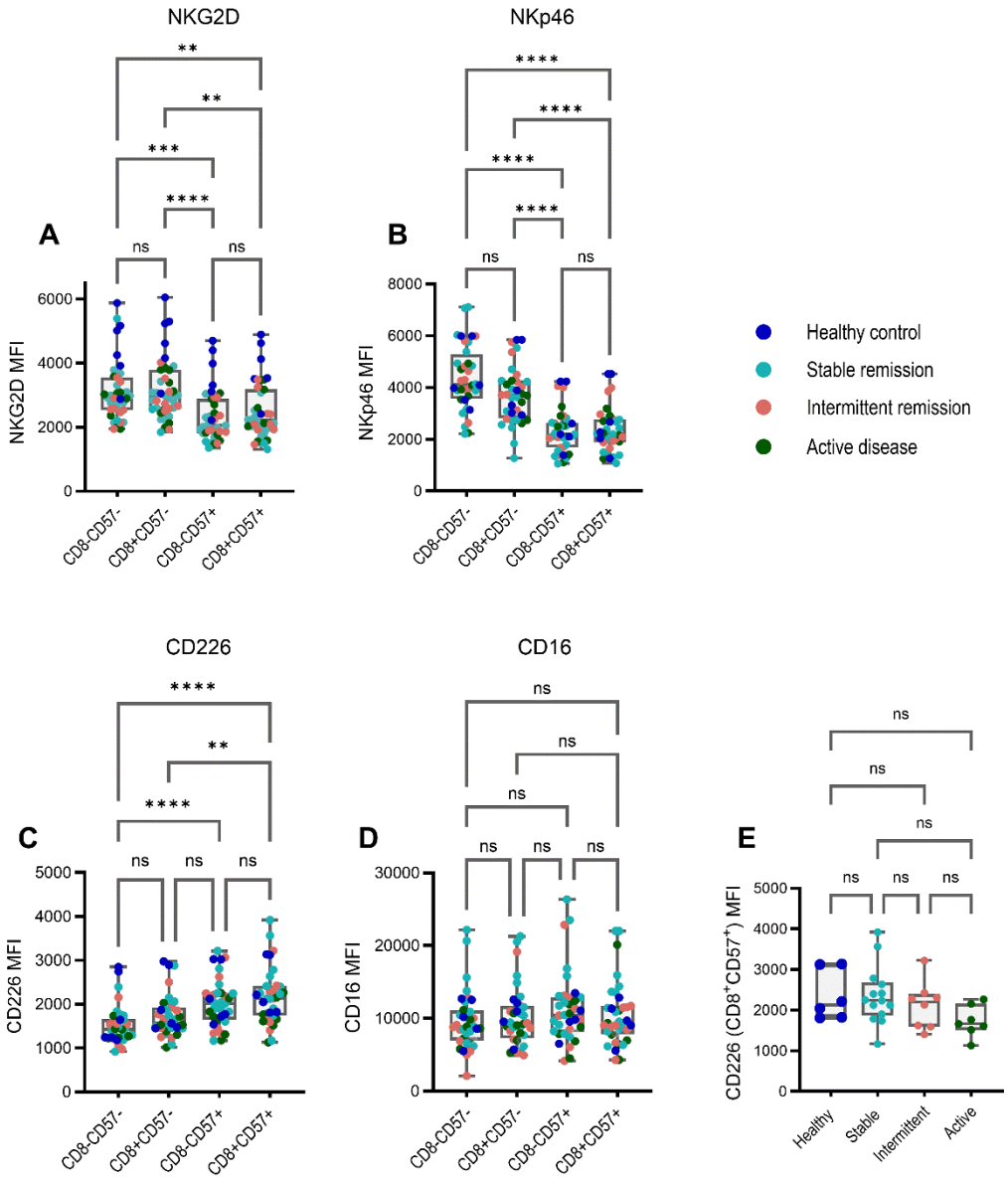

Figure 3. CD8+CD57+ NK cells display higher levels of CD226 expression consistent across RA disease activity states. (A-D) Median fluorescent intensity (MFI) of NKG2D, NKp46, CD226 and CD16 on NK cell subsets subdivided by CD8 and CD57 expression, (E) MFI of CD226 on $CD8^{+}CD57^{+}$ NK cells. Whiskers on plot represent min to max values. All P values were determined using the Kruskal-Wallis test with Dunns multiple test correction. *P <0.05, **P <0.01, P*** <0.001, P**** <0.0001

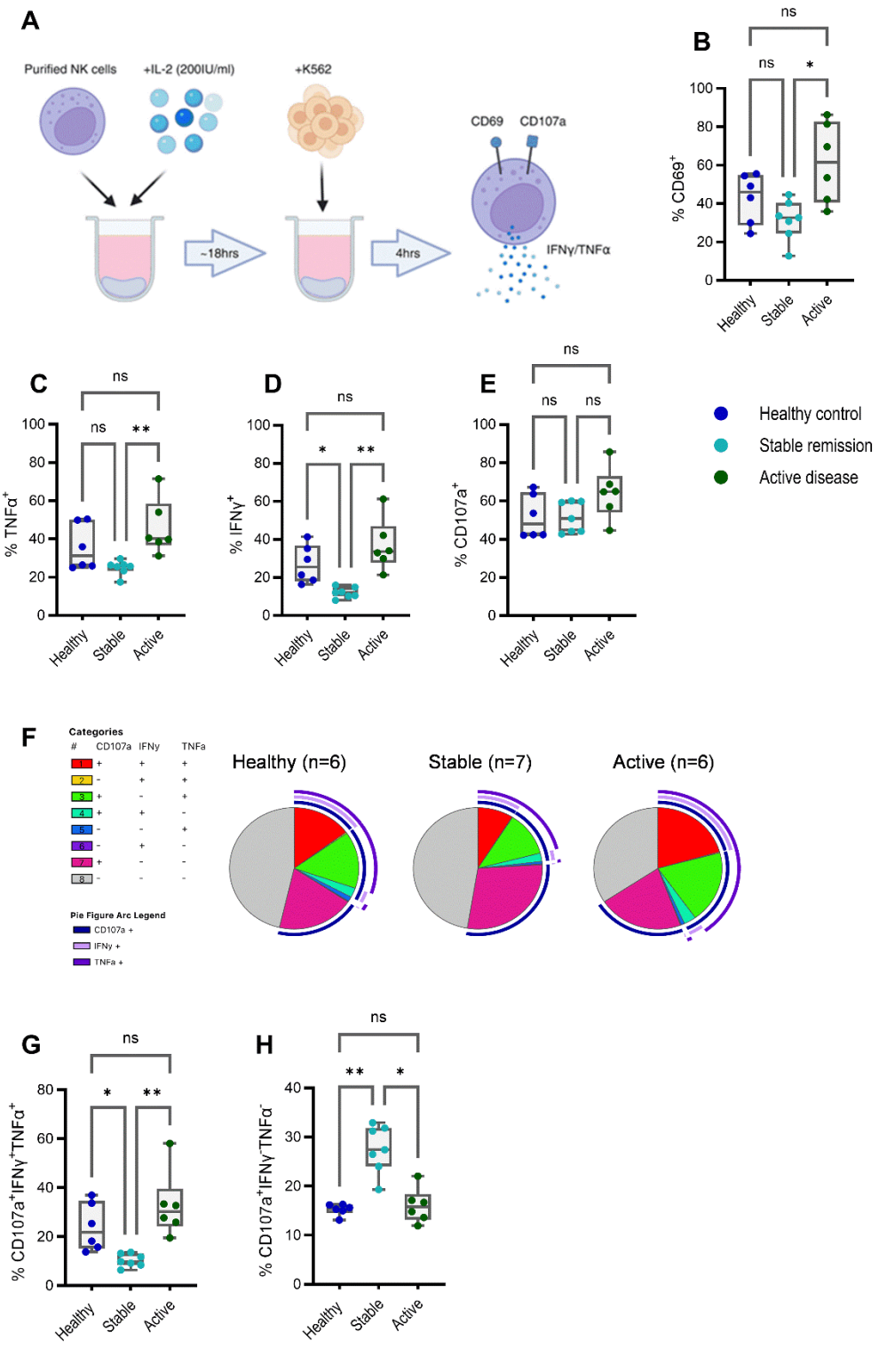
A
Purified NK cells
+IL-2 (200IU/ml)
+K562
~18hrs
4hrs
CD69
CD107a
IFNγ/TNFα
B
% CD69+
C
% TNFα+
D
% IFNγ+
E
% CD107a+
Healthy
Stable
Active
ns
Healthy control
Stable remission
Active disease
F
Categories
Pie Figure Arc Legend
CD107a +
IFNγ +
TNFα +
Healthy (n=6)
Stable (n=7)
Active (n=6)
G
% CD107a+IFNγ+TNFα+
H
% CD107a+IFNγ-TNFα-

Figure 4. NK cell subsets with normal degranulation responses and reduced pro-inflammatory cytokine expression are elevated in stable remission (A) NK cells from healthy donors (n=6), stable remission (n=7) and active disease (n=6) were purified and stimulated with IL-2 (200IU/ml) and incubated with K562 cells, (B-E) the proportions of NK cells expressing CD69, TNFα, IFNγ and CD107a, (F) SPICE analysis defines 8 distinct functional subtypes based on TNFα, IFNγ and CD107a expression, (G) the proportion of $CD107a^{+}IFN\gamma^{+}$ $TNF\alpha^{+}$ and (H) $CD107a^{+}$ $IFN\gamma^{-}TNF\alpha^{-}$ functional subsets. Whiskers on plots represent min to max values. All P values were determined using the Kruskal-Wallis test with Dunns multiple test correction. *P <0.05, **P <0.01.

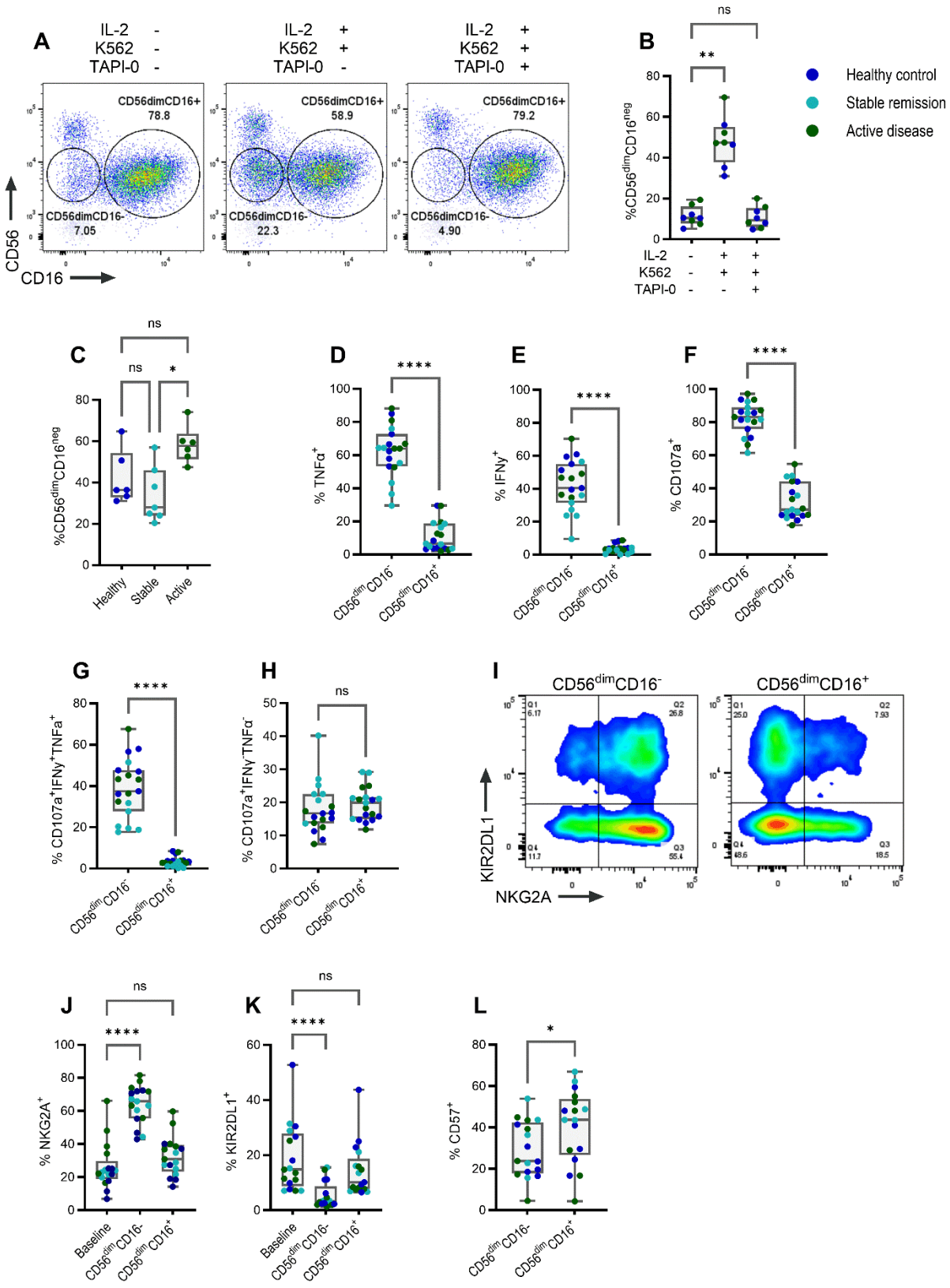
A
IL-2 - + +
K562 - + +
TAPI-0 - - +
CD56dimCD16+ 78.8
CD56dimCD16- 7.05
CD56dimCD16+ 58.9
CD56dimCD16- 22.3
CD56dimCD16+ 79.2
CD56dimCD16- 4.90
CD56
CD16
B
ns
**
%CD56dimCD16neg
IL-2 - + +
K562 - + +
TAPI-0 - - +
Healthy control
Stable remission
Active disease
C
ns
ns
*
%CD56dimCD16neg
Healthy
Stable
Active
D
****
% TNFα+
CD56dimCD16-
CD56dimCD16+
E
****
% IFNγ+
CD56dimCD16-
CD56dimCD16+
F
****
% CD107a+
CD56dimCD16-
CD56dimCD16+
G
****
% CD107a+IFNγ+TNFa+
CD56dimCD16-
CD56dimCD16+
H
ns
% CD107a+IFNγ-TNFα-
CD56dimCD16-
CD56dimCD16+
I
CD56dimCD16-
CD56dimCD16+
KIR2DL1
NKG2A
J
ns
****
% NKG2A+
Baseline
CD56dimCD16-
CD56dimCD16+
K
ns
****
% KIR2DL1+
Baseline
CD56dimCD16-
CD56dimCD16+
L
*
% CD57+
CD56dimCD16-
CD56dimCD16+

Figure 5. A distinct phenotypic subset of NK cells associated with *in vitro* polyfunctional responses is reduced in stable remission. (A-B) the *in-vitro* induction of a $CD56^{dim}CD16^{-}$ NK cell population, which arises in response to IL-2 stimulation and K562 interaction, is reduced upon treatment with TAPI-0 (5μM), (C) The proportion of $CD56^{dim}CD16^{-}$ NK cells in response to IL-2 stimulation and K562 interaction, (D-F) Comparison of the proportion of NK cells expressing TNFα, IFNγ, and CD107a as well as (G) $CD107a^{+}IFN\gamma^{+}$ $TNF\alpha^{+}$ and (H) $CD107a^{+}$ $IFN\gamma^{-}TNF\alpha^{-}$ functional subsets between $CD56^{dim}CD16^{-}$ and $CD56^{dim}CD16^{+}$ NK cells. (I) Representative flow plot demonstrating the expression of KIR2DL1 and NKG2A, (J-K) Differences in the expression from baseline ($IL\text{-}2^{-}K562^{-}$) of NKG2A, and KIR2DL1 between $CD56^{dim}CD16^{-}$ and $CD56^{dim}CD16^{+}$ subsets. (L) Comparison of the proportion of $CD57^{+}$ NK cells between $CD56^{dim}CD16^{-}$ and $CD56^{dim}CD16^{+}$ subsets. Whiskers on plots represent min to max values. All P values were determined using the Kruskal-Wallis test with Dunns multiple test correction. *P <0.05, **P <0.01, P**** <0.0001

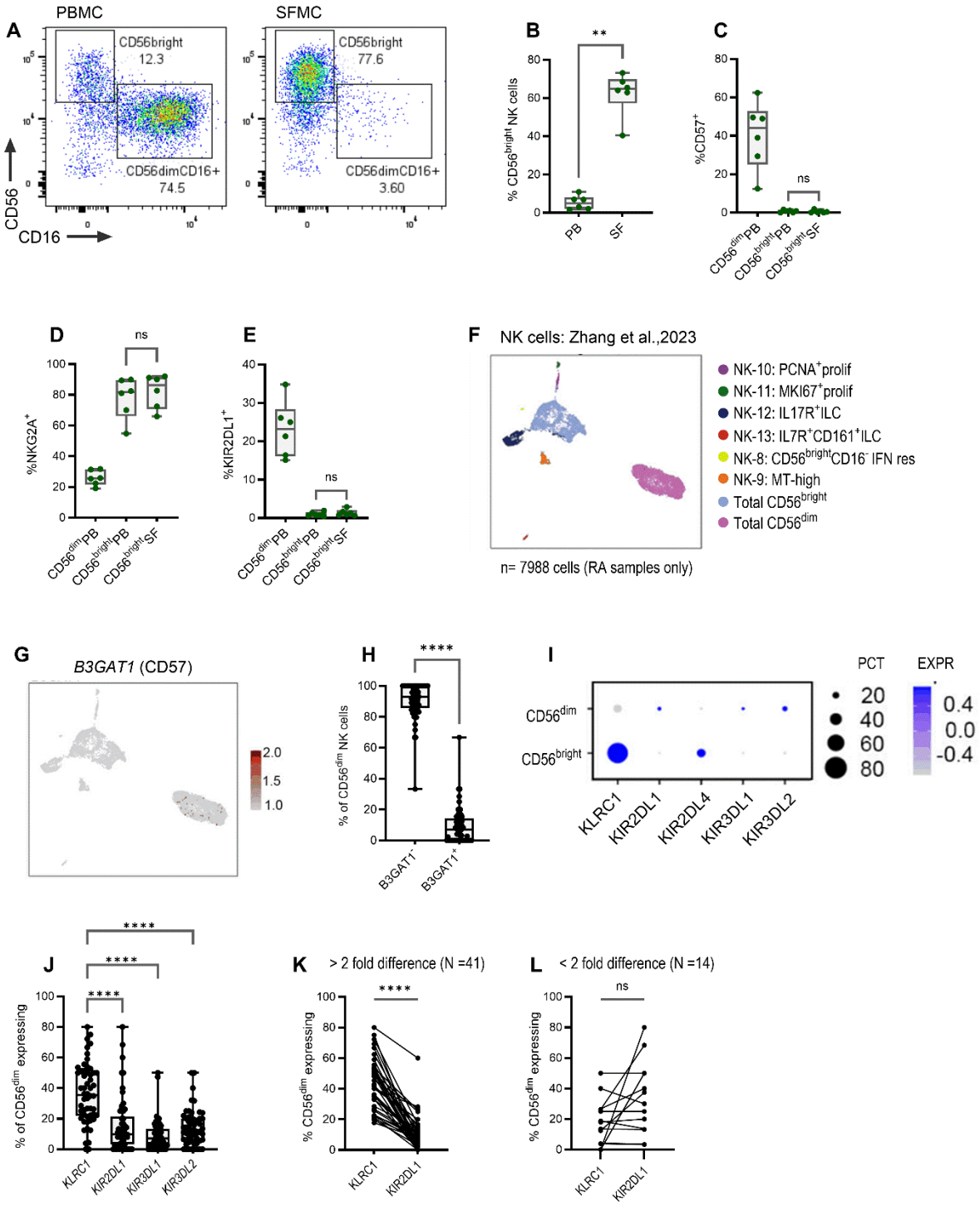
A
PBMC
SFMC
CD56bright
12.3
CD56dimCD16+
74.5
CD56bright
77.6
CD56dimCD16+
3.60
CD56
CD16
B
**
% CD56bright NK cells
PB
SF
C
%CD57+
ns
CD56dimPB
CD56brightPB
CD56brightSF
D
ns
%NKG2A+
E
%KIR2DL1+
ns
F
NK cells: Zhang et al.,2023
NK-10: PCNA+prolif
NK-11: MKI67+prolif
NK-12: IL17R+ILC
NK-13: IL7R+CD161+ILC
NK-8: CD56brightCD16- IFN res
NK-9: MT-high
Total CD56bright
Total CD56dim
n= 7988 cells (RA samples only)
G
B3GAT1 (CD57)
H
****
% of CD56dim NK cells
B3GAT1-
B3GAT1+
I
PCT
EXPR
CD56dim
CD56bright
KLRC1
KIR2DL1
KIR2DL4
KIR3DL1
KIR3DL2
J
****
% of CD56dim expressing
K
> 2 fold difference (N =41)
L
< 2 fold difference (N =14)
ns

Figure 6. Phenotypic features associated with sustained remission are reduced on NK cells from the joint of active RA. (A) Expression of CD56 and CD16 defines $CD56^{bright}CD16^{-}$ and $CD56^{dim}CD16^{+}$ subsets between paired peripheral blood (PB) and synovial fluid (SF) (N=6), (B) The proportion of $CD56^{bright}$ NK cells between PB and SF, (C-E) The expression of CD57, NKG2A and KIR2DL1 across $CD56^{dim}$ and $CD56^{bright}$ NK cells in PB and $CD56^{bright}$ NK cells in SF, (F) UMAP plot demonstrating 8 transcriptional NK Cell/ILC clusters derived from single cell RNA-Seq on synovial tissue from active RA patients, (G) UMAP feature plot showing the expression of *B3GAT1* across $CD56^{bright}$ and $CD56^{dim}$ clusters (H) Comparison of the proportion of $CD56^{dim}$ NK cells not expressing and expressing *B3GAT1* across individual tissue samples (n=63), (I) Bubble plots demonstrating the percentage of cells expressing genes for specific inhibitory receptors and their expression levels across $CD56^{bright}$ and $CD56^{dim}$ clusters, (J) Comparing the proportion of $CD56^{dim}$ NK cells expressing *KLRC1* to cells expressing genes encoding each corresponding KIR, (K-L) The proportion of NK cells expressing KLRC1 vs KIR2DL1 at a greater than or less than 2-fold difference. Whiskers on plots represent min to max values. All P values were determined using the Mann Whitney test (B-E, H), The Kruskal-Wallis test with Dunns multiple test correction (J), and the Wilcoxon matched-pairs signed rank test (K-L). **P <0.01, P**** <0.0001.

Table 1. Longitudinal DAS28 scores define remission groups

	DAS28-Baseline	DAS28-Month 3	DAS28-Month 6	DAS28-Month 9	DAS28-Month12
Stable remission					
Patient 1	*0.68 (REM)	0.49 (REM)	1.10 (REM)	0.97 (REM)	0.49 (REM)
Patient 2	*1.11 (REM)	0.63 (REM)	1.38 (REM)	0.72 (REM)	0.97 (REM)
Patient 3	*1.27 (REM)	0.95 (REM)	0.87 (REM)	1.65 (REM)	1.39 (REM)
Patient 4	*0.42 (REM)	0.15 (REM)	0.08 (REM)	0.08 (REM)	0.54 (REM)
Patient 5	*0.28 (REM)	0.98 (REM)	1.52 (REM)	1.17 (REM)	0.84 (REM)
Intermittent remission					
Patient 1	*2.07 (REM)	3.13 (LDA)	3.26 (MDA)	4.81 (MDA)	1.82 (REM)
Patient 2	*1.63 (REM)	4.19 (MDA)	4.19 (MDA)	2.74 (LDA)	2.05 (REM)
Patient 3	*2.06 (REM)	4.01 (MDA)	3.65 (MDA)	3.49 (MDA)	2.96 (LDA)
Patient 4	2.4 (REM)	*2.13 (REM)	3.12 (LDA)	4.61 (MDA)	3.68 (MDA)
Patient 5	2.90 (LDA)	3.54 (MDA)	4.92 (MDA)	3.44 (MDA)	*2.13 (REM)

Remission (REM) was defined as DAS28 <2.6, Low disease activity was defined as DAS28 >2.6 and <3.2, Moderate disease activity (MDA) was defined as DAS28 >3.2. *PBMC samples were selected at these timepoints for mass cytometry analysis

Table 2. Mass cytometry sample information

	Stable remission (n = 5)	Intermittent remission (n = 5)
Demographics		
Age in years, mean(SD)	60.40 (14.50)	59.60 (12.44)
Female/male, n (%)	3 (60) / 2 (40)	3 (60) / 2 (40)
Clinical parameters		
Disease duration in years, mean(SD)	3.3 (3.9)	2.6 (0.5)
DAS28, mean(SD)	0.75 (0.43)	2.6 (0.5)
VASP[A] in mm, mean(SD)	8 (7.6)	42 (34.5)
FACIT-F[B], mean (SD)	28.20 (22.19)	24.60 (23.09)
HAQ[C], mean (SD)	0.15 (0.3)	0.8 (0.8)
Swollen joint count, mean (SD)	0.2 (0.4)	1.2 (0.8)
Tender joint count, mean (SD)	0 (0)	0.4 (0.5)
Physician global assessment, mean (SD)	4 (8.9)	16 (11.4)
Patient global assessment, mean (SD)	12.80 (4.3)	39.80 (30)
Laboratory parameters		
ESR (mm/hr), mean (SD)	2.6 (1.8)	6.6 (3.2)
CRP (mg/dl), mean (SD)	5 (0)	4.3 (1.5)
Treatment information		

Methotrexate, n (%)	5 (100)	5 (100)
Hydroxychloroquine, n (%)	3 (60)	2 (40)
Sulfasalazine, n (%)	0 (0)	1 (20)
Leflunomide, n (%)	0 (0)	1 (20)

Demographics, clinical characteristics and treatment information relating to samples analysed in Figure 1A-D.

A Visual analogue scale for pain, B Functional Assessment of Chronic Illness Therapy- Fatigue, C Health assessment questionnaire